Journal of Materials Chemistry A RSCPublishing

ARTICLE

Proton Conductivity Enhancement in Oriented, Sulfonated Polyimide Thin Films

Cite this: DOI: 10.1039/xoxxoooooox

Karthik Krishnan,† Hiroko Iwatsuki,‡ Mitsuo Hara,‡ Shusaku Nagano,‡ and Yuki Nagao†,*

Received ooth January 2012,
Accepted ooth January 2012

DOI: 10.1039/xoxxoooooox

www.rsc.org/

Studies of proton transport in confined thin polymer electrolytes are essential for providing additional information regarding the structure–property relationships of such materials. Using a combination of proton transport measurements and structural characterization, we explored the effect of proton conductivity in sulfonated polyimide (SPI) under both bulk and nanostructured thin film systems. SPI film confined to a thickness of approximately 530 nm shows significant proton conductivity enhancement to a value of 2.6×10^{-1} S/cm (95% RH at 298 K), which is almost one order of magnitude more proton conductive than the bulk system (3.0×10^{-2} S/cm at 90% RH and 298 K). In thin film, the preferred chain packing along the in-plane direction can have considerable influence on the charge transport characteristics, which leads to the enhanced proton conductivity. The infrared (IR) p-polarized multiple-angle incidence resolution spectrometry (p-MAIRS) and in situ grazing-incidence small-angle X-ray scattering (GISAXS) were used to investigate the direction of polymer orientation and the changes in the internal polymeric structure under various humidity conditions, respectively. Under high-humidity conditions, the strong interaction between the side-chain sulfonic acid groups and water molecules causes an abrupt change in the internal structure in bulk SPI. Such structural rearrangement results in a liquid-crystal-like ordered polymer structure. The RH dependent FTIR−ATR studies reveal that, the accumulation of large fraction of water molecules with stronger hydrogen bonding at high humidity region causes the huge deviation in the internal morphology of the bulk samples.

1. Introduction

Aromatic polyimides have been widely investigated because of their high thermal stability, excellent chemical resistance, and favorable dielectric and gas permeability properties.[1] A polyimide (PI) functionalized with fluorinated and/or semialiphatic groups exhibits unique physical properties, which can be applicable to novel electronic and optical materials.[2–4] Recently, acid-functionalized or sulfonated polyimides (SPIs) have attracted interest as essential polymer electrolytes for fuel cells.[5,6] Because of their high molecular weights, the ease with which they can be formed into films, their enhanced proton conductivity, and high durability, SPIs have been used as possible substitutes for perfluorinated ionomer membranes.[7,8] However, proton conductivity, stability, and durability are still issues for SPIs because the sulfonated groups in the polymer electrolyte exhibit excessive swelling under fully hydrated conditions, which deteriorates their performance during fuel cell operation. Therefore, a number of structural investigations have been conducted to improve the proton conductivity and stability profiles of SPIs.[9,10] For example, Miyatake et al.[11] reported that the high proton conductivity of 1.67 Scm^{-1} (at 120 °C and 100% RH) is due to the high water-holding capability of the sulfonated polyimide containing fluorenyl groups. The strong interchain interaction among the polymer molecules allows for the dense packing of polymer chains, which reasons the possibility of stability under hydrated conditions, even at high temperatures. Notably, the properties of polymeric materials are not only influenced by their chemical modifications but also by the intermolecular aggregated structures that they form, such as the degree of chain packing and molecular ordering.

Conjugated polymer structures and the orientation of PI chains in thin films have been investigated because they significantly influence the resulting physical and chemical characteristics. For example, Terui et al.[12] have reported that, in the in-plane direction, highly oriented PI films exhibit a significant in-plane/out-of-plane birefringence property. In addition, the oriented PI membrane influenced the diffusion of gas molecules through the oriented skin layer, and the gas diffusive selectivity increased with the decrease in thickness of the skin layer.[13] In particular, polymer films confined to thicknesses that approach the characteristic length scale of the polymer can cause anisotropy in the orientation of polymer chains. This anisotropic polymer orientation is of particular importance because the majority of the electrical, mechanical, and optical properties of polymers depend on the degree of polymer chain orientation and the direction of orientation.[14,15] In general, the preparation method, solvent effect, annealing temperature, type of substrate, etc. are important parameters for obtaining the desired polymer orientation in thin films.[14–18] In recent years, numerous researchers have investigated the transport characteristics of polymer films in oriented molecular structures, because, during confinement, the self-assembled polymer structure exhibits a significant change in the proton transport characteristics relative to that of the bulk scale.[19–23]

In our previous studies,[24] we observed an enhancement of proton conductivity in highly oriented polypeptide structures on MgO(100) substrates, where the conductivity was nearly one order of magnitude greater than that of the bulk sample. In addition, the molecular orientation of the sulfonic acid groups significantly affects the proton transport property because the microphase separation, as well as the orientation of the proton-conductive groups, is an essential parameter for enhancing proton conductivity.[25] Typically, both the surface interaction that results from thin-film confinement and the wetting interactions between the substrate and the interface play an important role in the self-assembly of polymers. Proton conductivity and water uptake in confined systems largely depend on the surface properties of the substrate, the morphology of the thin films, the origin of interfacial effects, the alignment of domains, the domain spacing, etc.[26–31] The orientation of ionomer domains has already been reported to be influenced by the respective substrate wetting interactions.[32] For example, films cast on hydrophobic substrates display a parallel orientation of the ionomer channels, whereas films cast onto hydrophilic substrates exhibit an isotropic orientation. Consequently, the orientation of ionomer domains in a particular direction provides unique domain spacing in comparison with that of the bulk system, and this unique domain spacing causes the observed changes in the water uptake, swelling, and proton transport properties. However, a limited number of studies on the degree of the interfacial effect on proton transport characteristics have been reported. Both the change in polymer structure during confinement and the origin of the interfacial effect on polymer orientation are of fundamental interest in understanding the structure–property relationships of these materials.

In the present study, we describe the effect of proton conductivity on highly oriented SPI films prepared using the spin-coating technique. We employed a combination of p-MAIRS,[33,34] GISAXS, and impedance studies to investigate the proton transfer characteristics in the oriented polymer structures. We obtained clear evidence that the SPI films exhibit highly oriented polymer chains in the in-plane direction, with a slight polymer tilt in the backbone.

2. Experimental section

2.1. Materials

3,3'-Dihydroxybenzidine, propanesultone, and pyromellitic dianhydride (PMDA) were used as received from TCI, Japan. Acetic acid, acetic anhydride, methanol, and acetone were purchased from Wako Chemicals, Japan. Hydrochloric acid (Nacalai Tesque, Japan), sodium hydroxide (Kishida Chemical, Japan), m-cresol, and triethylamine (TEA) (Kanto Chemicals, Japan) were used as received.

2.2. Synthesis of SPI

Acetylation was initially performed using 3,3'-dihydroxybenzidine as the starting material because the amino groups in 3,3'-dihydroxybenzidine were protected by acetylation. In a typical reaction, 5 g 3,3'-dihydroxybenzidine was mixed with 1.5 ml acetic acid, 79 ml acetic anhydride, and 200 ml distilled water. This mixture was stirred at 70 °C for 1 hr. After the mixture cooled to room temperature, the precipitate was collected and separated using centrifugation. The products were washed several times with acetone to remove unreacted species, and the obtained precipitate was dried under vacuum. The incorporation of the acetyl functional group was confirmed by NMR analysis. Prior to each step, all of the prepared monomers were characterized by ^{1}H NMR.

Sulfonation of the acetylated 3,3'-dihydroxybenzidine was accomplished using 7.3 g propanesultone as the reagent. Thus, 2.4 g sodium hydroxide was dissolved in methanol (150 ml) and was added to the propanesultone mixture of acetylated 3,3'-dihydroxybenzidine. The reaction mixture was refluxed at 80 °C under an argon atmosphere for 6 hr. A pale-white precipitate was collected and washed several times with cold methanol. The obtained monomer was completely dissolved in distilled water, and an ion exchange process was performed using Amberlyst. Using a rotary vacuum evaporator, we separated the ion-exchanged monomers and dried them under vacuum. To remove the acetate groups, we added concentrated hydrochloric acid (HCl) to the final product obtained from the aforementioned step, and we subsequently refluxed the mixture at 120 °C for 1 hr under an inert atmosphere. After the mixture was refluxed, the cooled product was heated at 150 °C to evaporate the concentrated HCl. The HCl vapor was carefully neutralized with a concentrated base.

The sulfonated monomers (0.43 g) were polymerized with the required amount of PMDA (0.22 g), m-cresol (5 ml), and TEA (0.3 ml). m-Cresol was used as the solvent, and the polymerization reaction was conducted under an argon atmosphere at a constant temperature of 150 °C for 5 hr. The polymerized product was collected after being washed with cooled acetone. The final product was again subjected to an ion-exchange process using Amberlyst. GPC measurements were used to estimate the molecular weight of the prepared polymer, which was found to be 2.6×10^5.

2.3. Preparation of thin films

Nanostructured SPI thin films cast onto quartz substrates were prepared using an Active ACT−200 spin-coater. Prior to film deposition, each substrate was subjected to several cleaning processes, and plasma treatment was performed using a vacuum plasma system (Cute-MP; Femto Science, Korea) to improve surface hydrophilicity. The thicknesses of the thin films were measured using a surface profiler (KLA-Tencor P-15 profiler).

2.4. Conductivity measurements of the thin films

Proton conductivity was examined through impedance spectroscopy measurements using a Solartron 1260 frequency response analyzer equipped with a high-frequency Solartron 1296 dielectric interface. The relative humidity (RH) and temperature were established using a computer-controlled environmental test chamber (SH-221; Espec Corp). The conductivity measurements were performed at 298 K and at various RH values. For the thin film measurements, a two-probe method was employed to obtain the conductivity data. Gold contacts were used as the thin film electrodes for the conductivity measurements. The impedance data were collected between the frequency range of 1 Hz and 10 MHz, with an applied alternating potential of 50 mV. Thin-film conductivity (σ) was estimated by the following relation,

$$\sigma = \frac{d}{Rlt} \quad (1)$$

where d is the distance between the gold electrodes, R is the resistance value obtained directly from the impedance measurement, l is the length of the contact electrodes, and t is the thickness of the film.

2.5. p-Polarized multiple angle incidence resolution spectrometry (p-MAIRS)

p-MAIRS was used to investigate the polymer orientations of the nanostructured SPI thin films on Si wafers in both the in-plane and out-of-plane directions. The surface of the original Si wafer was oxidized before the measurement. The p-MAIRS measurements were collected with a Fourier-transform infrared (FTIR) spectrometer (Nicolet 6700; Thermo−Fisher Scientific) equipped with a mercury cadmium telluride (MCT) detector. Single-beam spectra were collected from 38° to 8° in 6° steps between the angle of incidence.

2.6. Grazing incidence small angle X-ray scattering (GISAXS)

GISAXS measurements were performed on a Rigaku FR-E X-ray diffractometer with an R-AXIS IV two-dimensional (2D) detector. The sample stage was composed of the goniometer and a vertical stage (CHUO Precision Industria ATS-C316-EM/ALV-300-HM) with a humidity-controlled cell. The cell had polyimide film (Kapton) windows and the humidity-controlled cell was obtained from BEL Japan. Nitrogen carrier gas was used as-received (without further dehumidification) from the gas cylinder to control the humidity. We used Cu Kα radiation (λ = 1.542 Å) with a beam size of approximately 300 μm × 300 μm, and the camera length was 300 mm. The incidence angle was chosen in the range from 0.18° to 0.22°. The diffraction patterns of the out-of-plane and in-plane directions that were obtained from thin film samples were used to extract information regarding the presence of liquid crystalline lamellar structures and the repeating unit of the polyimide main chain.

Small-angle X-ray scattering (SAXS) measurements in the bulk state were performed using the same X-ray diffractometer. A dry sample was placed in a capillary tube and was irradiated with the X-ray beam without further adjustments. In the case of the high-humidity condition, we placed both a portion of dry sample and a water droplet in the same capillary tube and then sealed it. After 2 days, we used the sealed capillary sample as the humid bulk state for SAXS measurements.

2.7. DFT calculations

Density functional theory (DFT) calculations were performed using the DMol3 package in Materials Studio v6.0.0 (Accelrys Software). The Perdew−Burke−Ernzerhof (PBE) function was chosen. The convergence threshold for the maximum force and maximum displacement for normal geometry optimization were set, respectively, to 0.02 Ha $Å^{-1}$ and 0.05 Å.

3. Results and discussion

3.1. Proton conductivity of SPI

This study illustrates the effect of proton conductivity on SPI at the bulk scale and in nanostructured thin film. Figure 1 shows the RH-dependent conductivity plots for both the bulk and thin-film materials. The proton conductivity of the thin film increases gradually and reaches a maximum value at 95% RH and 298 K; in addition, unlike the bulk SPI, the thin film does not exhibit a decrease in conductivity under this high-humidity condition. In the thin film, confinement effects are expected to play a vital role in the polymer orientation and transport properties. In RH dependent conductivity data, the maximum proton conductivity of the thin film is 2.6×10^{-1} S/cm (at 95% RH and 298 K). The conductivity of the pelletized bulk SPI (0.39 mm) reaches its maximum value of 3.0×10^{-2} S/cm at 90% RH and 298 K. Under high-humidity conditions, excessive swelling may accelerate the structural heterogeneity of the bulk sample, which causes a significant decrease in the conductivity. Hence, the proton conductivity of the thin film shows one order of magnitude higher than that of the pelletized bulk SPI.

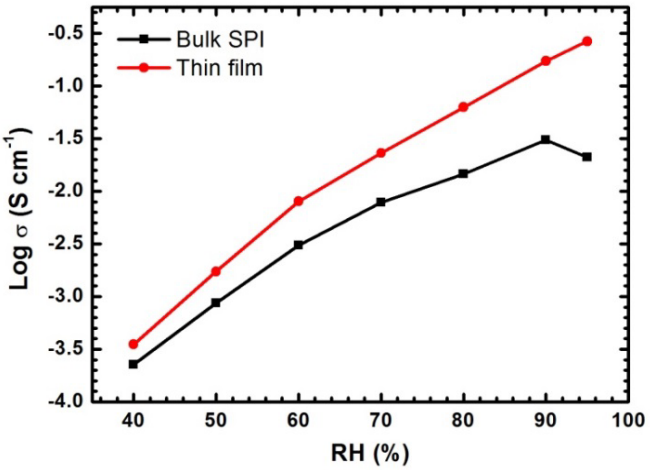

Fig. 1 Relative-humidity-dependent proton conductivity plots for the pelletized bulk SPI and thin film.

The Arrhenius plot of conductivity for the bulk SPI and thin film in the temperature range of 20-80 ºC is shown in Figure 2. The conductivity data were measured with a constant RH value of 90%. It is clearly seen that, the large deviation in the conductivity is obtained between the bulk SPI and thin film. The maximum proton conductivity of 2.8×10^{-1} S/cm is reached at 80 ºC in the thin film. This value is significantly higher than that of the bulk SPI (5.8×10^{-2} S/cm). The estimated activation energy values (E_a) for both the bulk SPI and thin film are 0.13 eV and 0.10 eV, respectively. This significant deviation in conductivities between the bulk SPI and nanostructured film has attracted and triggered further investigations into the internal structural characteristics of the thin film. The observation that the thin film confinement affect strongly enhances the proton conductivity of this material is particularly important.

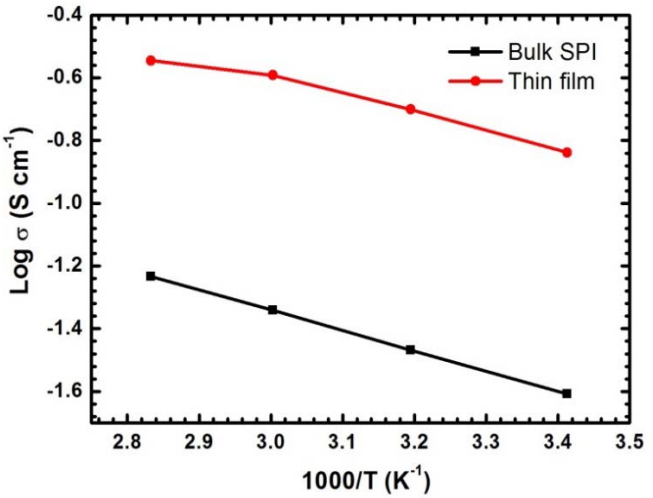

Fig. 2 Temperature-dependent proton conductivity plots for the bulk and thin SPI film.

We speculate that an ordered molecular orientation and confinement effects in thin films are most likely able to induce proton transport properties. However, not much report to date is available for the relationship between polymer orientation and proton transport behavior in a confined thin film. Hence, we have performed a more detailed structural analysis of the SPI thin film to obtain a more complete understanding of the associated structure–property relationships.

3.2. Evaluation of SPI orientation by p-MAIRS

Infrared p-MAIR spectroscopy is an important tool for the investigation of molecular orientation in thin films. The measured in-plane (IP) and out-of-plane (OP) p-MAIR spectra of the SPI thin film are shown in Figure 3. In the IR spectra, three strong vibrational modes are observed at 1381, 1504, and 1726 cm^{-1}. The band at 1381 cm^{-1} is due to the C−N−C bond of the imide groups, and the mode at 1504 cm^{-1} is attributed to the phenyl C−C stretching vibration. The two vibrational modes at 1726 and 1781 cm^{-1} correspond to the C=O asymmetric and symmetric stretching vibrations of imide groups, respectively.[35] The orientation dynamics in confined systems are determined according to the change in intensity profiles of p-MAIR spectra. Typically, the strongest absorbance arises when the electric field vector of the IR rays and the orientation of the molecular vibration are parallel.[36]

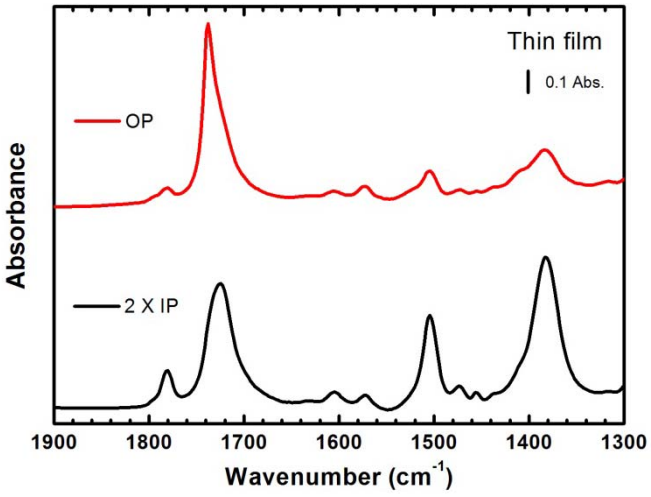

Fig. 3 Infrared p-MAIR spectra for the SPI thin film, measured from 38° to 8° in steps of 6°.

Accordingly, the absorbances of the IP vibrational modes of C−N−C and phenyl C−C are two times more intense than the absorbance of the OP component, suggesting that the SPI thin film is highly oriented parallel to the substrate plane. Moreover, a notable finding is obtained from the C=O asymmetric and symmetric stretching modes in the IP spectrum. The peak strength of the asymmetric vibrational mode is significantly reduced relative to that of the OP component. Simultaneously, the symmetric stretching of the IP component is more prominent than that of the OP component. On the basis of these two stretching modes, the asymmetric stretch has a dipole moment that is directed normal to the backbone, whereas the symmetric stretch has a dipole moment that falls along the backbone direction. This result indirectly indicates a small degree of polymer tilting or that the molecule protrudes from the surface toward the normal direction, thereby causing the reduction of the asymmetric peak intensity in the IP spectra.[35]

To gain further insight into the effect of the C=O asymmetric mode in the OP direction, the presence of band shifts in the absorption spectrum must be considered. The appearance of peak shifts in a vibrational spectrum can be attributed to the influence of physical and chemical contributions. In the present OP spectra, the asymmetric vibrational mode is significantly shifted to higher positions (1735 cm^{-1}) relative to that of the IP component (1726 cm^{-1}). The observation of this shift in peak position and intensity profile correlates with the occurrence of the tilted polymer symmetry or the surface-perpendicular C=O component.[37] This p-MAIRS study provides quantitative support for the earlier assumption of the relationship between SPI orientation and proton transport behavior in conductivity analysis.

For the pelletized bulk SPI, the FTIR-ATR measurement was used along the three orthogonal directions, and the characteristic vibrational modes are shown in Figure 4. As a result of the random orientation of the bulk material, the maximum absorbance in the vibrational mode is limited as compared with the oriented thin film; hence, the bulk SPI exhibits the same observance strengths in all three directions. In addition, a significant frequency downshift is observed for both the C−N−C (1376 cm^{-1}) and C=O asymmetric (1720 cm^{-1}) stretching vibrational modes.

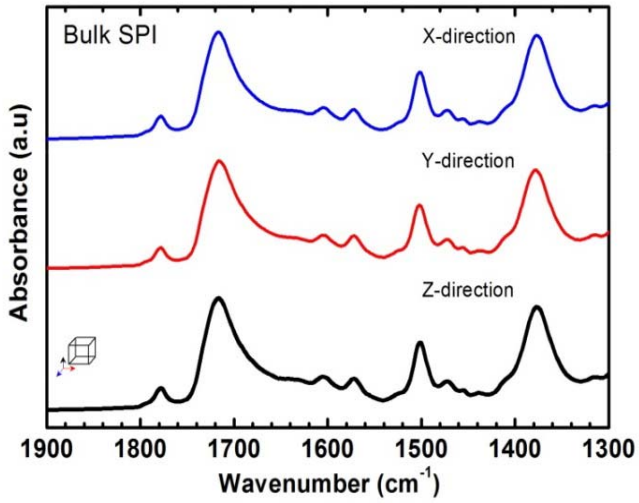

Fig. 4 FTIR-ATR spectra for the pelletized bulk SPI, measured in the three orthogonal directions.

3.3. Structural analysis using GISAXS

To explain the change in internal structure and/or morphological characteristics of the thin film, in situ GISAXS measurements were conducted (Figure 5) for the SPI thin film under various humidified conditions. Figure 5 (a, b) represents the 2D GISAXS profiles for the SPI thin film, taken from 0% RH to 95% RH. Under conditions of increasing humidity, the 2D scattering pattern clearly demonstrates the origin of the new scattering arc (the white arrow in Figure 5b). The 1D GISAXS profiles of both the in-plane and out-of-plane directions for SPI thin film are shown in Figure 5 (c, d). Under the 95% RH condition, two scattering intensity at 0.37 and 0.28 $Å^{-1}$ (q_y) are observed in the in-plane direction (Figure 5c). The corresponding d-spacing values for these two peaks are 1.6 and 2.2 nm, respectively. The 1D GISAXS patterns for the out-of-plane direction show the peak shift toward the smaller-angle direction (q_z from 0.39 to 0.34 $Å^{-1}$, Figure 5d), suggesting that the expansion of the out-of-plane structure is the result of water uptake under the high RH range.

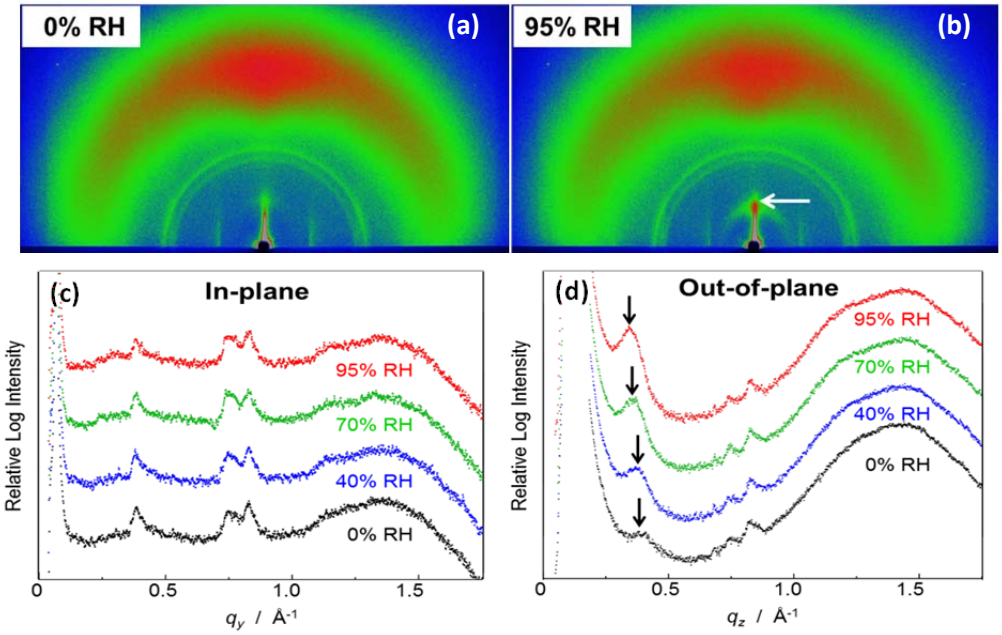

Fig. 5 (a, b) The 2D GISAXS patterns at 0% RH and 95% RH, respectively, and the humidity-dependent 1D GISAXS profiles in the (c) in-plane and (d) out-of-plane directions of the SPI thin film.

The appearance of scattering intensity at approximately 0.75 and 0.84 Å^{-1} (q_y) corresponds to the diffraction pattern of the reference film (Kapton) used during the GISAXS measurements.

PIs possess rigid and planar molecular structures that are oriented parallel to the substrate plane and exhibit mixed aggregated structures, such as liquid-crystal-like and ordered crystalline structures.[38] Therefore, the in-plane scattering peaks correspond to the periodic length of the repeating units in the ordered structure. To estimate the repeating unit of the primary chain, a DFT calculation was performed. The rod-like molecular structure of SPI was investigated, yielding the periodic distance value that is shown in Figure 6. The periodic unit almost matches the experimental d-spacing values of 1.6 and 2.2 nm (q_y = 0.37 and 0.28 Å^{-1}, respectively). We propose that the ordered structure of SPI films is the driving state, as described below. SPI backbones aggregate in the in-plane direction with bridging of the sulfonated alkyl side chain to the out-of-plane direction, forming a lamellar structure parallel to the substrate. With increasing humidity, the sulfonated interlamellar spacing is selectively hydrated. Consequently, the in-plane high-conductivity behavior is attained by the expansion of the interlamellar proton conduction path into the out-of-plane direction. These behaviors are essentially identical to that of the lamellar phase of the lyotropic liquid crystal (LC) system.[39]

Figure 7 shows the SAXS pattern for bulk SPI, measured under both dry and high-relative-humidity conditions. The obtained results give more information regarding the significant change in internal structure of SPI under the high-relative-humidity condition. The scattering intensity of q= 0.41 Å^{-1} (d = ca. 1.4 nm) under the dry condition is an overlapping peak that occurs due to the repeating unit of the main chain and the dried lamella phase in the partially ordered domains. Under the high-humidity condition, the emergence of a stronger intensity at approximately 0.21 Å^{-1} (q) is evident in the diffraction pattern, confirming the highly ordered lamellar phase as the major diffraction peak following the water uptake expansion behavior. The corresponding d-spacing value (2.9 nm) for this peak is very large. The expanded ordered lamella structure can be interpreted as a resulting lyotropic LC-like phase, which arises as a result of the strong interaction between the sulfonic acid side chain units and water molecules, as well as the hydrophobic packing of the PI main chains.

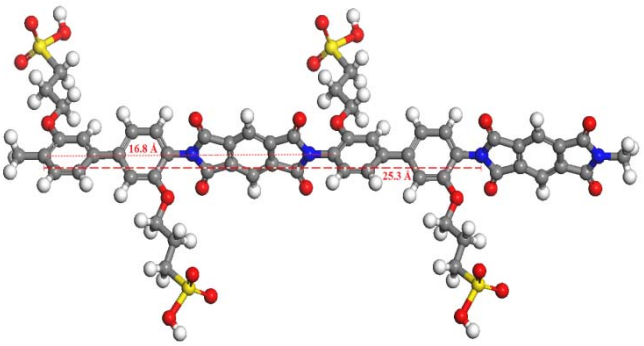

Fig. 6 The DFT geometrical analysis performed for a rod-like SPI backbone and the obtained mean inter-distance values.

In comparison with the case of the high-humidity region, the observed new small-angle peak originates from the lyotropic ordered domains, in which the ch-packing[38] of the neighboring SPI chains is highly ordered in the out-of-plane direction. The strong structural rearrangement that occurs at the bulk scale is due to the vigorous translation motion of sulfonic side groups during the high-humidity exposure. Similarly, other authors have proposed that the vigorous motion of SPI chains can induce molecular rearrangement during thermal imidization as a result of the bent molecular structures.[38] Possibly, the bent (or twisted) molecular structure is also essential for the enhancement of the packing order of SPI chains under the high-relative-humidity condition, which supports the interpretation of a highly orientated liquid-crystalline-like order in the bulk case. From these observations, the molecular rearrangement due to structural instability clearly increases when the system approaches the bulk scale.

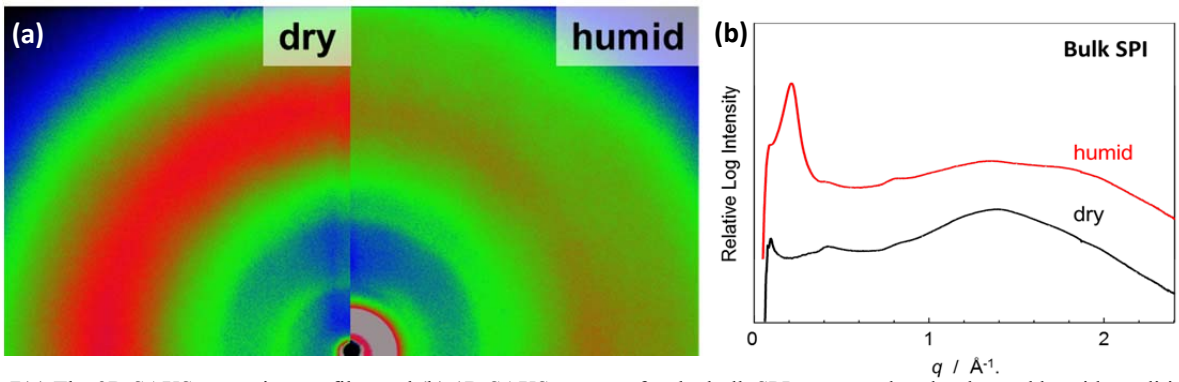

Fig. 7(a) The 2D SAXS scattering profiles and (b) 1D SAXS patterns for the bulk SPI, measured under dry and humid conditions.

As indicated by the preceding GISAXS results, the inherent anisotropic lyotropic lamella structure parallel to the substrate plane is formed in the thin film. Occurrence of this inherent in-plane polymer orientation might be due to the spin coating technique as a result of the centrifugal force applied during spinning.[40] The surface energy of the substrate may also influence the interfacial interaction between the polymer chains and the polymer orientation along the surface parallel in a film.[41–43] Consequently, the oriented structure can have a significant advantage in in-plane conduction behavior because the in-plane-oriented lamellar structure constructs the long-range continuous proton conduction paths with the sulfonic layers. On the other hand, the bulk state does not exhibit this anisotropic structure. The isotropic multi-oriented domain cannot lead to long-range pathways. On the basis of the previous discussion, the highly oriented lyotropic lamellar structure enhances the proton conductivity in comparison with that in the bulk by expanding the proton conduction pathways.

3.4. Humidity-dependent FTIR−ATR studies

We attempted to analyze the change in the internal structure of the polymer under various RH conditions using FTIR-ATR measurements.[44] This approach is more quantitative and provides additional support to our previous discussion. Figure 8 shows the RH-dependent FTIR-ATR spectra of the pelletized bulk SPI system. In the pelletized bulk SPI, the observed broad band between 3000 and 3720 cm^{-1} corresponds to the OH stretching vibration of water molecules. The absorbance of the OH stretching mode increases gradually up to 70% RH. When the system reaches RH values of 80% and greater, the absorbance of OH traces increases significantly. More importantly, the new peak at 1637 cm^{-1} is observed in the high-humidity region, corresponding to the bending frequency of water molecules. According to the unique physical state of water molecules, the bending frequency can vary from 1630 to 1670 cm^{-1}.[45] The appearance of a band between 1630 and 1645 cm^{-1} corresponds to a pure state of liquid water. In association with the change in absorbance and frequency values, a frequency downshift can be observed from 95% RH (1637 cm^{-1}) to 70% RH (1633 cm^{-1}). The difference in the vibrational mode can be interpreted as a result of the change in hydrogen bonding strength within the system. Notably, the bending frequency of water molecules in the higher wavenumber region is assigned to the characteristics of strong hydrogen bonding, whereas the frequency downshift in this same region is ascribed to the weaker hydrogen bonding of water molecules.[45–47] The result obtained at RH greater than 90% is unexpected and interesting with respect to understanding the changes in internal morphology of the pelletized bulk SPI. The accumulation of a significant fraction of water molecules with stronger hydrogen bonding results in a prominent deviation in the internal morphology of the bulk samples, which causes more intense absorption peaks in the entire spectrum. The appearance of the bending frequency of water molecules in the FTIR-ATR spectra further supports the interpretation presented in the previous discussion of the strong structural reconstruction in the randomly ordered pelletized bulk SPI, following the decrease in conductivity at higher humidity region.

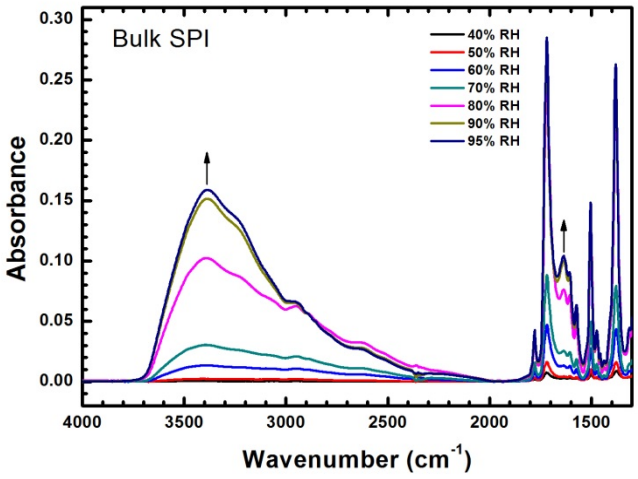

Fig. 8 An observation of the OH traces using FTIR-ATR spectra of the pelletized bulk SPI under various humidity conditions.

RH-dependent FTIR-ATR measurements were also conducted on SPI thin film (Figure 9). In the present spectra there are three distinct characteristic bands have been observed: the first in the region between 3600 and 3400 cm^{-1} is due to the contemporary presence of water molecules stretching ν_3 and ν_1. The interpretation of the band between 3300 and 3200 cm^{-1} includes the overtone of water bending. The third band at approximately 3060 cm^{-1} is possibly a combination and overtone of the matrix.[45] All these bands demonstrate the linear relationship between the OH absorbance value and the relative humidity. Because of the nanoscale dimensionality of the thin film, the intensity of this band is not similar to that of the pelletized bulk SPI. The structural alteration is minimally apparent in the fully hydrated region; in addition, a limited increase in the intensity of the 1637 cm^{-1} mode corresponding to the OH bending vibration is evident. This result provides indirect evidence of the fact that the abrupt change in internal structure is restricted when the system is confined as a thin film. The primary polymer orientation in the in-plane direction also limits further changes in internal structure under

the higher humidity condition. The peak observed between 2250 and 2400 cm^{-1} corresponds to the stretching of O=C=O molecular vibrations present in atmospheric air. These results also suggest that the higher proton conductivity observed in the SPI thin film is due primarily to the greater ordering of the polymer chain orientations, which is accompanied by high structural stability.

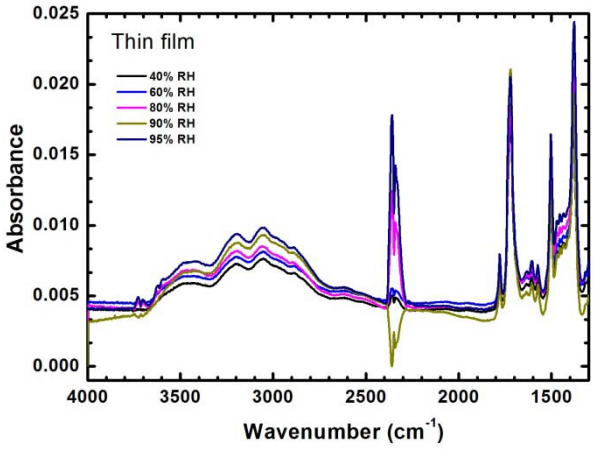

Fig. 9 An observation of the OH traces in the SPI thin film using FTIR-ATR measurements.

4. Conclusions

The effect of polymer orientation on the transport properties of SPI was investigated using a wide range of structural analysis methods. We have demonstrated that the thin film confinement effect significantly affects the polymer orientation and proton-conducting properties of SPI. In SPI thin film, the inherent anisotropic lyotropic lamellar structure falls parallel to the substrate plane and develops long-range continuous proton-conducting paths, which is in contrast to observations for the bulk case. Thus, the observed proton conductivity value of SPI thin film exhibits one order of magnitude greater than that of the bulk sample. In the bulk case, an abrupt change in internal structure as a result of the increased hydrogen bonding behavior of the water molecules results in a sudden decrease in the conductivity value at RH values greater than 90%. The p-MAIRS measurements used in this study represent an important tool for determining the changes in internal structure of polymer films. Based on the p−MAIR spectra, the polymer orientation of SPI is highly ordered in the in-plane direction. The existence of a small degree of polymer tilting or the surface-perpendicular C=O component is evidenced by the combination of a change in the peak intensity and a peak shift in the out-of-plane component. The in situ GISAXS diffraction profile reveals a significant deviation in the internal symmetry of polymer chains under high-humidity conditions. Because of the strong interaction between the sulfonic acid side chain units and water molecules, the structures of PI chain packing, including the more ordered domains, can be interpreted as a lyotropic LC-like phase. On the basis of the diffraction profiles, the degree of lyotropic LC-like order increases in the bulky molecular structure because the ch-packing between the contiguous PI chains orders more rapidly in the out-of-plane direction due to excessive water absorption. Humidity-dependent FTIR-ATR studies of both the bulk and thin SPI samples also support the observation of changes in internal polymer structure. Under high-humidity conditions, the emergence of a new peak at 1637 cm^{-1} and the increase in peak intensities indicate that strong structural alterations dominate within the bulk sample. Consequently, this work demonstrates that the interfacial confinement of polymer structures significantly influences the proton transport characteristics.

Acknowledgments

This work was supported in part by the Nanotechnology Platform Program (Molecule and Material Synthesis) of the Ministry of Education, Culture, Sports, Science and Technology (MEXT), Japan. This work was financially supported by the Japan Society for the Promotion of Science (JSPS) through the Funding Program (GR060) for Next Generation World-Leading Researchers (NEXT Program), initiated by the Council for Science and Technology Policy (CSTP).

Author information

Corresponding author

*ynagao@jaist.ac.jp Phone: +81(Japan)-761-51-1541

Notes and references

1 C. E. Sroog, *J. Polym. Sci.: Macromol. Rev.*, 1976, **11**, 161–208.
2 M. Hasegawa, Y. Shindo, T. Sugimura, S. Ohshima, K. Horie, M. Kochi, R. Yokota and I. Mita, *J. Polym. Sci. Part B*, 1993, **31**,1617–1625.
3 T. Matsuura, S. Ando, S. Sasaki and F. Yamamoto, *Macromolecules*, 1994, **27**, 6665–6670.
4 M. Sato, Y. Nakamoto, K. Yonetake and J. Kido, *Polym. J.*, 2002, **34**, 601–607.
5 X. Guo, J. Fang, T. Watari, K. Tanaka, H. Kita and K. Okamoto, *Macromolecules*, 2002, **35**, 6707–6713.
6 K. Miyatake, H. Zhou and M. Watanabe, *Macromolecules*, 2004, **37**, 4956–4960.
7 K. Miyatake, T. Yasuda, M. Hirai, M. Nanasawa and M. Watanabe, *J. Polym. Sci.: Part A: Polym. Chem.*, 2007, **45**, 157–163.
8 K. Miyatake, T. Yasuda, M. Watanabe, *J. Polym. Sci.: Part A: Polym. Chem.*, 2008, **46**, 4469–4478.
9 Y. Yin, J. Fang, T. Watari, K. Tanaka, H. Kita and K. I. Okamoto, *J. Mater. Chem.*, 2004, **14**, 1062–1070.
10 N. Asano, K. Miyatake and M. Watanabe, *Chem. Mater.*, 2004, **16**, 2841–2843.
11 K. Miyatake, H. Zhou and M. Watanabe, *Macromolecules*, 2004, **37**, 4956–4960.
12 Y. Terui and S. Ando, *J. Polym. Sci., Part B*, 2004, **42**, 2354–2366.
13 M. Niwa, H. Kawakami, T. Kanamori, T. Shinbo, A. Kaito and S. Nagaoka, *Macromolecules*, 2001, **34**, 9039–9044.
14 J. Ma, K. Hashimoto, T. Koganezawa and K. Tajima, *J. Am. Chem. Soc.*, 2013, **135**, 9644–9647.
15 P. Dhar, P. P. Khlyabich, B. Burkhart, S. T. Roberts, S. Malyk, B. C. Thompson and A. V. Benderskii, *J. Phys. Chem. C*, 2013, **117**, 15213–15220.
16 X. T. Hao, T. Hosokai, N. Mitsuo, S. Kera, K. K. Okudaira, K. Mase and N. Ueno, *J. Phys. Chem. B*, 2007, **111**, 10365–10372.
17 C. Daniel, A. Avallone, P. Rizzo and G. Guerra, *Macromolecules*, 2006, **39**, 4820–4823.
18 T. Uekusa, S. Nagano and T. Seki, *Macromolecules*, 2009, **42**, 312–318.
19 Y. Aoki, K. Ogawa, H. Habazaki, T. Kunitake, Y. Li, S. Nagata and S. Yamaguchi, *Chem. Mater.*, 2010, **22**, 5528–5536.
20 Y. Daiko, K. Katagiri and A. Matsuda, *Chem. Mater.*, 2008, **20**, 6405–6409.

21 J. Maier, *Nat. Mater*., 2005, **4**, 805–815.
22 V. V. Belousov, *J. Eur. Ceram. Soc*., 2007, **27**, 3459–3467.
23 D. K. Paul, A. Fraser, J. Pearce and K. Karan, *ECS Trans*., 2011, **41**, 1393–1406.
24 Y. Nagao, J. Matsui, T. Abe, H. Hiramatsu, H. Yamamoto, T. Miyashita, N. Sata and H. Yugami, *Langmuir*, 2013, **29**, 6798–6804.
25 Y. Nagao, *J. Phys. Chem. C*, 2013, **117**, 3294–3297.
26 G. C. Abuin, M. C. Fuertes and H. R. Corti, *J. Membr. Sci*., 2013, **428**, 507–515.
27 S. K. Dishari and M. A. Hickner, *ACS Macro Lett*., 2012, **1**, 291–295.
28 Z. Siroma, R. Kakitsubo, N. Fujiwara, T. Ioroi, S. I. Yamazaki and K. Yasuda, *J. Power Sources*, 2009, **189**, 994–998.
29 P. W. Majsztrik, M. B. Satterfield, A. B. Bocarsly and J. B. Benziger, *J. Membr. Sci*., 2007, **301**, 93–106.
30 Q. A. Zhao, P. Majsztrik and J. Benziger, *J. Phys. Chem. B*, 2011, **115**, 2717–2727.
31 S. A. Eastman, S. Kim, K. A. Page, B. W. Rowe, S. Kang and C. L. Soles, *Macromolecules*, 2012, **45**, 7920–7930.
32 M. A. Modestino, D. K. Paul, S. Dishari, S. A. Petrina, F. I. Allen, M. A. Hickner, K. Karan, R. A. Segalman and A. Z. Weber, *Macromolecules*, 2013, **46**, 867–873.
33 T. Hasegawa, *J. Phys. Chem. B*, 2002, **106**, 4112–4115.
34 T. Hasegawa, *Anal. Chem*., 2007, **79**, 4385–4389.
35 J. Sung, D. Kim, C. N. Whang, M. Oh-e and H. Yokoyama, *J. Phys. Chem. B*, 2004, **108**, 10991–10996.
36 T. Hasegawa, *Anal. Bioanal. Chem*., 2007, **388**, 7–15.
37 M. Matsunaga, T. Suzuki, K. Yamamoto and T. Hasegawa, *Macromolecules*, 2008, **41**, 5780–5784.
38 J. Wakita, S. Jin, T. J. Shin, M. Ree and S. Ando, *Macromolecules*, 2010, **43**, 1930–1941.
39 J. C. P. Gabriel, F. Camerel, B. J. Lemaire, H. Desvaux, P. Davidson and P. Batail, *Nature*, 2001, **413**, 504–508.
40 K. Kurabayashi and K. E. Goodson, J. Appl. Phys., 1999, **86**, 1925–1931.
41 M. Bass, A. Berman, A. Singh, O. Konovalov and V. Freger, Macromolecules, 2011, **44**, 2893–2899.
42 M. Bass, A. Berman, A. Singh, O. Konovalov and V. Freger, J. Phys. Chem. B, 2010, **114**, 3784–3790.
43 J. A. Dura, V. S. Murthi, M. Hartman, S. K. Satija and C. F. Majkrzak, Macromolecules, 2009, **42**, 4769–4774.
44 (a) Prior to each measurement, the sample was maintained at 298 K and under the specified humidity condition for 30 min. Each measurement was performed within 10 s of the sample being removed from the humidity chamber. Compared with the conventional gravimetric method, this measurement technique simultaneously provides the relationship between water uptake capability and the perturbed internal geometry of polymers in different humidity conditions. Furthermore, the spectroscopic method can offer in situ information about chemical reactions, such as polymer restructuring, and/or physical interactions (e.g., hydrogen bonding) between polymers and diffusants.44b,44c On the basis of the intensity variations of OH traces in the FTIR-ATR spectra, the water-uptake capability and structural information is observed for both bulk and thin SPIs. (b) I. Linossier, F. Gaillard, M. Romand and J. F. Feller, *J. Appl. Polym. Sci*., 1997, **66**, 2465–2473. (c) F. Sundfors, T. Lindfors, L. Hofler, R. Bereczki and R. E. Gyurcsanyi, *Anal. Chem*., 2009, **81**, 5925–5934.
45 M. Laporta, M. Pegoraro and L. Zanderighi, Phys. Chem. Chem. Phys., 1999, **1**, 4619–4628.
46 T. A. Ford and M. Falk, *Can. J. Chem*., 1968, **46**, 3579–3586.
47 S. Quezado, J. C. T. Kwak and M. Falk, *Can. J. Chem*., 1984, **62**, 958–966.